Applied Catalysis B: Environmental 302 (2022) 120870

Contents lists available at ScienceDirect

Applied Catalysis B: Environmental

journal homepage: www.elsevier.com/locate/apcatb

Direct production of ethanol with high yield from glycerol via synergistic catalysis by Pd/CoO_x and Cu/SBA-15

Jianfeng Shan [a,b,*], Yanfeng Xue [c], Dengfeng Wang [a], Zheng Chen [a], Shanhui Zhu [b,**]

[a] College of Chemistry, Chemical Engineering and Materials Science, Zaozhuang University, Zaozhuang, Shandong 277160, PR China
[b] State Key Laboratory of Coal Conversion, Institute of Coal Chemistry, Chinese Academy of Sciences, 27 South Taoyuan Road, Taiyuan, Shanxi 030001, PR China
[c] Institute of Interface Chemistry and Engineering, Department of Chemistry and Chemical Engineering, Taiyuan Institute of Technology, Taiyuan, Shanxi 030008, PR China

ARTICLE INFO

Keywords:
Glycerol
Hydrogenolysis
Ethanol
Pd/CoO_x
Cu/SBA-15

ABSTRACT

Direct hydrogenolysis of glycerol to ethanol in liquid phase was studied for the first time in this work, and the results showed that Pd/CoO_x gave high ethanol selectivity and good reusability. The reaction pathways were thoroughly investigated, and it was found that ethanol was mainly produced by consecutive hydrogenolysis of glycerol with 1,2-propanediol as intermediate. More importantly, PdCo alloy was identified as the main active site for ethanol production from glycerol by in situ XRD, TEM, H_2-TPR, XPS and controlled experiments. Remarkably, Cu/SBA-15 was employed as co-catalyst to adjust the reaction routes and inhibit Pd/CoO_x aggregation. By synergistic catalysis of Pd/CoO_x and Cu/SBA-15, the yield of ethanol then reached to 84.5%, which is the highest value ever reported in glycerol hydrogenolysis reactions.

1. Introduction

During the last decade, the booming biodiesel industry led to an oversupply of by-produced glycerol [1,2]. Although glycerol is widely used in cosmetics, pharmaceuticals, and tobacco industry, its small market requirement cannot keep glycerol price from falling [3–5]. Conversion of glycerol to some high value-added chemicals is a good way to improve profitability of biodiesel industry. On this background, selective production of acrolein [6,7], 1,2-propanediol/1,3-propanediol [8–13], monomers [14], allyl alcohol [15], glycidol [16], some esters [17,18] and acids [19,20] by catalytic conversion of glycerol have been widely investigated and reported in previous literatures, and a small quantity of ethanol has been detected in a few related reports [21–25].

Ethanol is an important chemical product popularly used in medicines, drinks, and foods [26,27]. Besides, it has been used as fuel additive in America and Brazil from last century. China has also started a nationwide application of ethanol gasoline, which will lead to a rapid increase in ethanol consumption [28–30]. At present, ethanol is mainly produced by microbial fermentation of cereals and hydration of ethylene from petrochemical industry [26,27]. To guarantee food security and alleviate the depletion of fossil resources, ethanol production from surplus glycerol can be a good option and this process may have a wide application prospect because of biodiesel production continuing to increase. As predicted by Mota et al. [31], ethanol price could decrease by about 40% if glycerol is used for its commercial production.

Ethanol production from glycerol by microbial fermentation has been widely reported in the literatures [32–37]. Compared to fermentation, catalysis is more efficient in many cases. However, before the year 2018, ethanol was only reported as a by-product with very low selectivity in catalytic conversion of glycerol. In 2015, Hutchings et al. [23] reported that glycerol could be converted to methanol with 60% selectivity on MgO, and ethanol was also produced with a selectivity lower than 5%. Yang et al. [24] showed that Ag decorated commercial Raney Ni catalyst exhibited better selectivity to C_3 products than unmodified Raney Ni catalyst, and ethanol derived from C—C bond cleavage was also detected. Ryneveld et al. [22] found that the selectivity to ethanol over Ni/SiO_2 improved with rising reaction temperature and reached 20.2% at 320 °C. These enlightening works indicate a strong possibility of the selective formation of ethanol from glycerol.

In 2018, Hou et al. [28] first reported that Ni-substituted stichtite derived $Ni_{2.4}/Mg_{3.7}Cr_{2.0}O_{6.7}$ catalyst could directly produce ethanol with a selectivity of 63.3% from glycerol at 250 °C in the gas-phase. Soon the same group discovered that Co/ZnO catalyst synthesized from CoZn-ZIF showed excellent activity and selectivity (57.9%) for the

* Corresponding author at: College of Chemistry, Chemical Engineering and Materials Science, Zaozhuang University, Zaozhuang, Shandong 277160, PR China.
** Corresponding author.
E-mail addresses: shan_jianfeng@foxmail.com (J. Shan), zhushanhui@sxicc.ac.cn (S. Zhu).

https://doi.org/10.1016/j.apcatb.2021.120870
Received 27 August 2021; Received in revised form 11 October 2021; Accepted 27 October 2021
Available online 1 November 2021

direct production of ethanol at lower temperature in a fixed-bed reactor [29]. More recently, excellent work was done by Kostyniuk's group [30]. Ethanol was produced from glycerol by direct cracking at 350 °C. The maximum ethanol selectivity reached up to 99.6 mol% over 20 wt% CsZSM-5 with GHSV = 625 h^{-1} after 2 h on stream. However, the catalyst experienced a rapid deactivation because of coking, and the overall ethanol yield was lower than 60%. Above researches sufficiently demonstrated that glycerol can be converted to ethanol with high selectivity in the gas-phase. However, to our knowledge, the data is lacking on liquid-phase catalytic conversion of glycerol with ethanol as main product until now. In comparison to gas-phase reactions, liquid-phase reactions performed in batch or semi-batch reactors are more convenient to use with less investment, especially for high boiling point reactants at high pressure. In this research work, liquid-phase glycerol hydrogenolysis to ethanol tests were performed with Pd, Pt, and Ru based catalysts because of their high activity in C—C bond cleavage, and various carriers were evaluated. Of all the tested catalysts, Pd/CoO_x catalyst prepared by co-precipitation reached the best catalytic performance. Furthermore, the reaction pathways of glycerol to ethanol over Pd/CoO_x catalyst was thoroughly investigated, and PdCo alloy was identified as the main active site by various characterizations and controlled experiments. More importantly, ethanol yield was greatly boosted to as high as 84.5% by adjusting the reaction routes with the assistance of Cu/SBA-15, and this is the highest value reported in glycerol hydrogenolysis reactions so far.

2. Experimental

2.1. Catalyst preparation

Pd/CoO_x was prepared by a co-precipitation method. Typically, palladium chloride ($PdCl_2$, 60% palladium) was dissolved in hydrochloric acid, and a certain amount of cobalt nitrate hexahydrate ($Co(NO_3)_2{\cdot}6H_2O$, purity ≥ 99%) was then added. After that, an aqueous solution of Na_2CO_3 (1 mol L^{-1}) was added dropwise into the metal salt solutions at 40 °C with continuous stirring, with the pH value of the resulting solution being controlled at about 9. The solid was filtered, washed with deionized water, and dried at 80 °C in a vacuum oven for eight hours. The obtained catalyst was calcined at 300 °C for six hours. Pd/CeO_2, Pd/NiO_x, Pd/FeO_x, Pd/Al_2O_3, Pt/CoO_x, Ru/CoO_x catalysts were prepared by the same method. Pd/Co_2O_3-IM and Pd/C-IM catalysts were prepared by incipient wetness impregnation. For these catalysts, a solution of palladium chloride in hydrochloric acid was added to each support. Co_2O_3 was synthesized by the same procedure of preparing Pd/CoO_x without addition of palladium chloride. Activated charcoal was purchased from Sigma-Aldrich as well as other reagents used in this work. For Pd/Co_2O_3-IM, the following drying and calcination processes were the same with Pd/CoO_x. Unlike other catalysts, the dried Pd/C-IM was calcined with protection of nitrogen. For all supported noble metal catalysts, the nominal noble metal loading was 3 wt%. Cu/SBA-15 was prepared by simple grinding with a nominal Cu loading of 10 wt%, which has been reported in our previous research [5]. The detailed synthesis procedures are described in the Supplementary Material.

2.2. Characterization

The actual Pd, Pt, and Ru loadings were determined by inductively coupled plasma atomic emission spectroscopy (ICP-AES) on a Thermo iCAP6300 instrument. N_2 physisorption measurements were conducted to get the specific surface area of different catalysts with a TriStar3020 II gas adsorption analyzer. X-ray diffraction (XRD) measurements were performed on a D8 Advance X-ray diffractometer. The transmission electron microscopy (TEM) images, high-resolution TEM (HRTEM) images, high-angle annular dark-field scanning TEM (HAADF-STEM) images and energy dispersive spectrometer (EDS) mapping were taken by a FEI Tecnai G2F20 transmission electron microscope. The X-ray photoelectron spectra (XPS) were measured on a Thermo ESCALAB 250 instrument equipped with a monochromatic Al Kα ($h\nu$ = 1486.6 eV) source. H_2 temperature-programmed reduction (H_2-TPR) measurements were performed with a Micromeritics AutoChem II 2920 chemisorption analyzer. Scanning electron microscopy (SEM) images and the corresponding EDS mapping were obtained by field emission scanning electron microscope (FESEM, JSM 7001-F). The detailed procedures of XRD, TEM, HR-TEM, HAADF-STEM, XPS, and H_2-TPR can be found in the Supplementary Material.

Cu/SBA-15 was also characterized by XRD, H_2-TPR and TEM with the same instruments described above.

2.3. Catalytic test

Direct hydrogenolysis of glycerol to ethanol reactions were carried out in a 25 mL Teflon-lined stainless-steel autoclave. Before every test, the catalyst was prereduced in a 10 vol% H_2/Ar flow (40 mL min^{-1}) at selected temperature for 2 h. After cooling down to room temperature, the catalyst was transferred to a solution of glycerol (10 wt% in deionized water or 1-propanol, 10 g) without exposure to air. Then the reactor was sealed, purged with H_2 (99.9%), pressurized with hydrogen (3.0 MPa) and finally heated to the target temperature. After every test, the reactor was put in a dry ice/acetone bath and cooled to − 60 °C.

In a two-step method, glycerol (10 wt% in 1-propanol, 10 g) was first converted to 1,2-propanediol over Cu/SBA-15 under 3.0 MPa H_2 in a 25 mL Teflon-lined stainless-steel autoclave. After that, Cu/SBA-15 was separated by centrifuge, and the obtained solution was applied to further hydrogenolysis over Pd/CoO_x in the same reactor.

The reusability of Pd/CoO_x and Pd/FeO_x was tested in glycerol hydrogenolysis reaction. After every reaction, the catalyst was separated by filtration, dried at 100 °C, ground with a mortar and pestle, and then calcinated in air at 300 °C, followed by reduction under a 10 vol% H_2/Ar flow at 250 °C. The regeneration procedures of the mixed catalysts (Pd/CoO_x + Cu/SBA-15) were similar to that of pure Pd/CoO_x, but without the grinding step.

The gas phase was analyzed by an Aglient 7890A gas chromatograph equipped with a thermal conductivity detector (TCD) and two flame ionization detectors (FID) to determinate the amount of CH_4, CO_2, etc. The liquid phase was analyzed on a Shimadzu GC-2010 Plus gas chromatograph equipped with a FID, an HP-PONA capillary column (I.D. = 0.20 mm, length = 50 m), and an autosampler. The external calibration method was applied to determine remaining reactants and products. Glycerol conversion was calculated by Eq. (1). Selectivity and yield of ethanol (EtOH), 1-propanol (NPA), ethylene glycol (EG) and 1,2-propanediol (1,2-PDO) was calculated by Eqs. (2) and (3):

$$\text{Glycerol conversion} = \frac{\text{moles of reacted reactant}}{\text{moles of reactant in the feed}} \times 100\% \quad (1)$$

$$\text{Product selectivity} = \frac{\text{moles of a defined product}}{\text{moles of reacted reactant}} \times 100\% \quad (2)$$

$$\text{Product yield}^1 = \frac{\text{moles of a defined product}}{\text{moles of reactant in the feed}} \times 100\% \quad (3)$$

Eq. (4) was used to get the yield of methanol (MeOH):

$$\text{Product yield}^2 = \frac{\text{moles of methanol}}{\text{moles of carbon atom in reactant}} \times 100\% \quad (4)$$

The yield of CO_2 and CH_4 was obtained by Eq. (5):

$$\text{Product yield}^3 = (1\text{-selectivity of products in liquid phase}) \times \text{glycerol conversion} \times \text{molar ratio of } CO_2 \text{ or } CH_4 \text{ in gas phase} \times 100\% \quad (5)$$

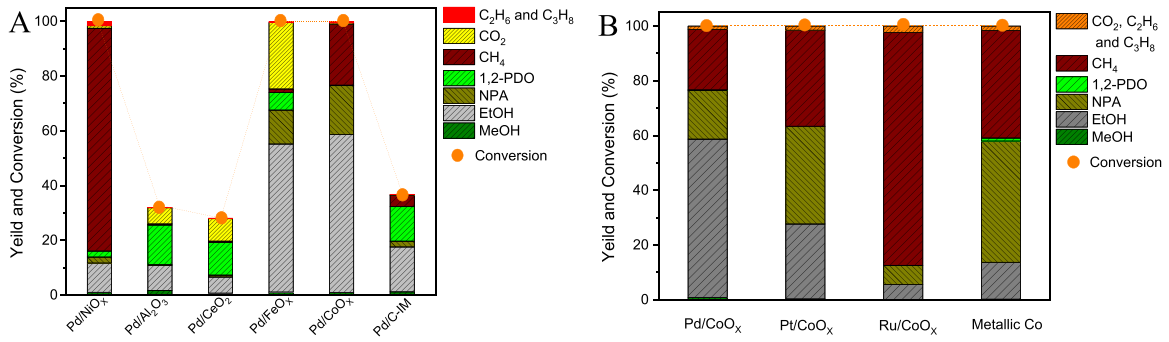

Fig. 1. Catalytic performance of hydrogenolysis of glycerol. (A) Pd, Pt, and Ru on CoO_x; (B) Pd on different oxides and metallic Co (Co_2O_3 reduced at 350 °C). Reaction conditions: 0.25 g catalyst (before reduction), 1.0 g (10.9 mmol) glycerol, 9 g water, 3 MPa H_2, 25 h, 230 °C.

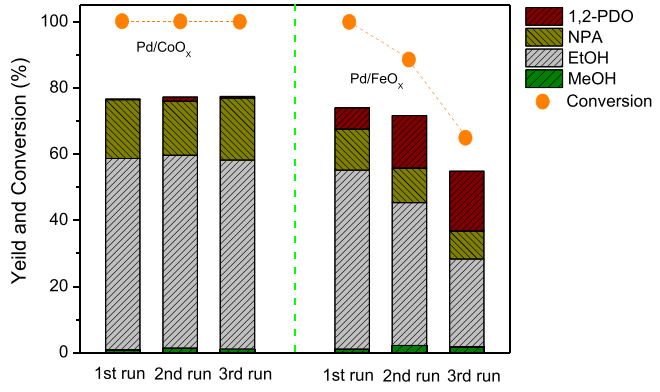

Fig. 2. Reusability of Pd/CoO_x and Pd/FeO_x. Reaction conditions: 0.25 g catalyst (before reduction), 1.0 g (10.9 mmol) glycerol, 9 g water, 3 MPa H_2, 25 h, 230 °C.

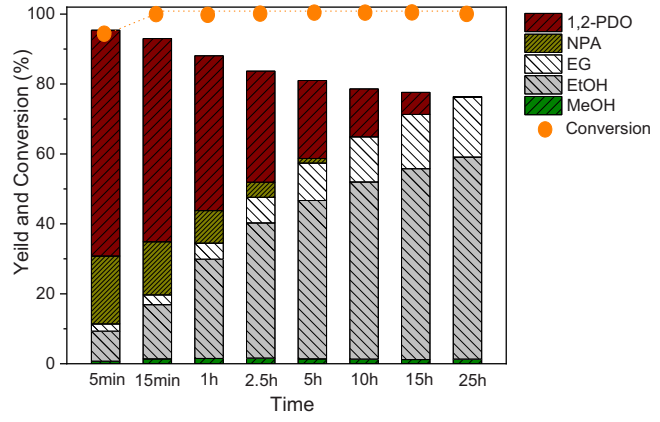

Fig. 3. Effect of reaction time on glycerol conversion and liquid-phase products yield. Reaction conditions: 0.25 g catalyst (before reduction), 1.0 g (10.9 mmol) glycerol, 9 g water, 3 MPa H_2, 25 h, 230 °C.

3. Results and discussion

3.1. Catalytic performance of supported noble metal catalysts and the reaction pathways over Pd/CoO$_x$

As seen from Fig. 1, all tested catalysts can convert glycerol to ethanol at the given condition. However, only Pd/CoO_x and Pd/FeO_x showed high selectivity over 50% for ethanol with 100% conversion. Pd/CoO_x gave the highest ethanol yield (57.8%), and the monohydric alcohol (methanol, ethanol and 1-propanol) selectivity achieved 76.5%, which is also higher than other catalysts. The high selectivity to ethanol might be ascribed to the moderate C–C cleavage ability of Pd/CoO_x. Although the products in liquid-phase were mainly ethanol, 1-propanol and 1,2-propanediol over the tested catalysts, the gas-phase products were very different. The main gaseous product was carbon dioxide (> 90%) on Pd/Al_2O_3, Pd/CeO_2, and Pd/FeO_x catalysts in this research, whereas methane constituted more than 95% of the gaseous products when Pd/CoO_x, Ru/CoO_x, Pt/CoO_x, Pd/Ni_2O_3, Pd/C-IM and metallic Co catalyzed this reaction at the same conditions. The detailed liquid-phase product distributions are listed in Table S1. It has been noted that metals with strong adsorptive properties readily catalyze the formation of methane from hydrocarbons by exhaustive hydrogenolysis [38,39], thus leading to high methane selectivity on Pd/CoO_x, Ru/CoO_x, Pt/CoO_x, Pd/Ni_2O_3, Pd/C-IM, and metallic Co. Especially, Ni and Ru based catalysts have been thoroughly studied in methanation reactions and shown high reactivity [40–42]. Taken together, the ultra-high selectivity to methane on Pd/NiO_x and Ru/CoO_x can be explained.

Fig. 2 illustrates the conversion of glycerol and the yield of liquid products in different reaction runs. For Pd/CoO_x, no obvious decrease in reactivity and ethanol selectivity can be seen after three catalytic cycles. In the case of Pd/FeO_x, glycerol conversion decreased from 100% to 66% during three catalytic cycles, and ethanol yield dropped significantly at the same time. It should be noted that some red sediments appeared after the products solution being exposed to air overnight when Pd/FeO_x was employed as catalyst. However, the just-separated products solution was transparent and nearly colorless. Because carbon dioxide was the main product in gas-phase after glycerol hydrogenolysis on Pd/FeO_x, the catalyst was probably corroded by carbonate solution due to dissolution of carbon dioxide in water at the reaction temperature. For Pd/CoO_x, similar phenomena were not observed as the primary gaseous product was methane, which might result in better stability than Pd/FeO_x.

In summary, Pd/CoO_x was the only sample that exhibited high ethanol selectivity and good reusability, and the reaction pathways was further studied for glycerol hydrogenolysis on this sample. Fig. 3 clearly shows the changes of glycerol conversion and liquid-phase products yield over time on Pd/CoO_x catalyst, and the specific data can be found in Table S2. As can be seen, glycerol can be easily converted under the reaction conditions. After the reaction temperature rising to 230 °C, glycerol conversion reached 100% in 15 min. At this point, the main product was 1,2-propanediol (58.1%), and the yield of ethanol was only 15.5%. As reaction time was prolonged, 1,2-propanediol and ethylene glycol were gradually consumed, accompanied by the formation of ethanol and 1-propanol, as shown in Fig. 3. After 25 h reaction, ethanol yield reached 57.8%. Thus, two reaction pathways for ethanol production are reasonably to be deduced from the dependency of product distribution on reaction time: (1) C—C bond of glycerol was cracked for ethylene glycol production, and ethanol was then obtained by C—OH bond cleavage in ethylene glycol; (2) glycerol was firstly converted to 1,2-propanediol, and ethanol was subsequent produced by cleavage of

Table 1
Catalytic performance of Pd/CoO_x with different reactants.

Reactant	Time	Conv. (%)	Yield (%)							Carbon balance (%)
			MeOH	EtOH	EG	NPA	1,2-PDO	CH_4	Others	
MeOH	5 h	77.3	–	–	–	–	–	75.7	1.6	92.2
EtOH	5 h	1.4	0.2	–	–	–	–	1.0	0.2	98.8
NPA	5 h	1.1	–	0.2	–	–	–	0.6	0.3	98.3
1,2-PDO	15 min	14.7	0.1	12.5	0.3	1.3	–	0.4	0.1	96.5
	2 h	28.6	0.3	22.6	–	3.3	–	2.1	0.3	97.1
	20 h	99.2	0.2	66.4	–	22.3	–	9.5	0.8	96.3
EG	5 h	70.5	5.3	20.6	–	–	–	43.3	1.3	93.3

Reaction conditions: 0.25 g catalyst (before reduction), 32.6 mmol for MeOH and 10.9 mmol for other reactants, 9 g water, H_2 3 MPa, 230 °C.

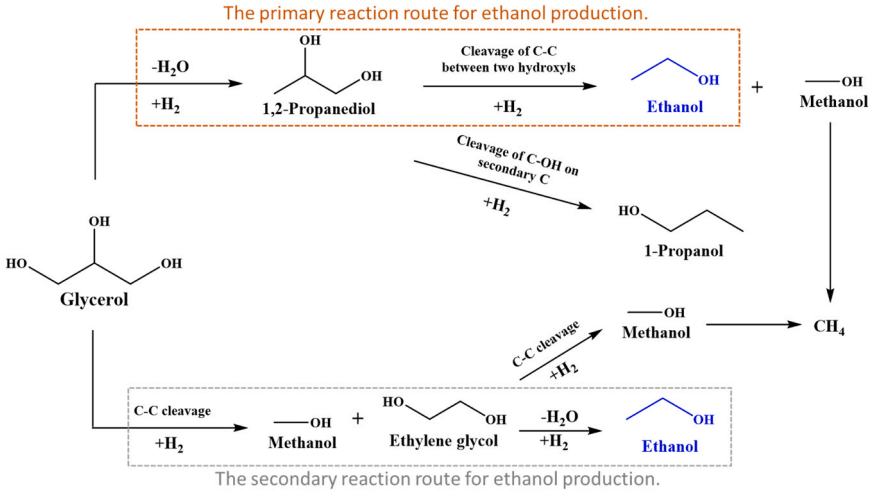

Scheme 1. Reaction pathways for liquid-phase hydrogenolysis of glycerol on Pd/CoO_x.

the C—C bond between two hydroxyl-linked carbon atoms in 1,2-propanediol.

To prove the ethanol production pathways proposed above, 1,2-propanediol, ethylene glycol, 1-propanol, ethanol and methanol were employed separately as reactants with Pd/CoO_x as catalyst at the same conditions. The catalytic results are presented in Table 1. The selectivity of methane is 97.9% for methanol conversion after 5 h, indicated that almost all methanol was converted to methane. Ethanol and 1-propanol showed very low reactivity on Pd/CoO_x catalyst, and the conversion were just 1.4% and 1.1%, respectively. For 1,2-propanediol, the products in liquid-phase were primarily ethanol and 1-propanol. After 20 h at 230 °C, the yield of ethanol reached as high as 66.4%, and 1-propanol yield was 22.3%. When ethylene glycol was used, the yield of ethanol (20.6%) was much lower than that of methane (43.3%). For all the tests listed in Table 1, methane was the main ingredient in gas-phase products. These results indicate that 1,2-propanediol is the primary intermediate product in glycerol hydrogenolysis to ethanol on Pd/CoO_x, while ethylene glycol should be the secondary intermediate product for ethanol formation. The main formation pathways of detected products are illustrated in Scheme 1.

3.2. Catalyst characterizations

The surface area and the metal loading of Pd/Pt/Ru of different catalysts are listed in Table S1. For catalysts with Co_2O_3 as carrier, no great difference can be in observed in surface area. Besides, the actual metal loadings are similar in all catalysts.

Fig. 4 shows the XRD patterns of in situ hydrogen reduced Co_2O_3 and Pd/CoO_x. In Fig. 4A, after 2 h reduction at 230 °C, the XRD pattern of reduced Co_2O_3 showed diffraction peaks of CoO at 36.3°, 42.3° and 61.4° (PDF-#48-1719), indicating the incomplete reduction of Co_2O_3 at this temperature. For the XRD pattern of Co_2O_3 reduced at 350 °C, the characteristic peak of CoO disappeared and the diffraction peaks of Co appeared (PDF#15-0806), implying that Co_2O_3 was completely reduced to metallic Co. It should be noted that three diffraction peaks could be found at 41.5°, 44.3° and 47.2° for Pd/CoO_x reduced at 230 °C, and no CoO diffraction peak was observed. The peak at 44.3° is assigned to the (1 1 1) lattice plane of metallic Co (PDF#15-0806), suggesting that Co_2O_3 could be reduced to metallic Co at 230 °C when Pd was introduced. That is, Pd can promote the reduction of Co_2O_3.

The standard 2θ values corresponding to the (1 1 1) and (2 0 0) plane diffraction of Pd were indicated by the black dashed lines located at 40.1° and 46.7° in Fig. 4A. Compared to pure Pd, two diffraction peaks in the XRD pattern of Pd/CoO_x reduced at 230 °C shifted to the higher angels (41.5° and 47.1° peaks in Fig. 4A), because the incorporation of Co into the Pd crystal lattice induced the contraction of Pd lattice [43,44]. This result suggests the formation of PdCo alloy in Pd/CoO_x catalyst, consistent well with former reports [44–46]. Fig. 4B illustrates the influence of reduction temperature on the XRD patterns of Pd/CoO_x catalyst. With the rising heating temperature, all diffraction peaks became better defined. At the same time, the diffraction peaks of PdCo alloy shifted to higher angle direction, as displayed in Fig. 4C. This phenomenon indicates that more Co atoms incorporated to the Pd crystal lattice with the increase in reduction temperature, which means an increase in the degree of alloying between Pd and Co [38,46].

HR-TEM and HAADF-STEM analyses were conducted for further investigation of Pd/CoO_x structure. As shown in Fig. 5A, interplanar spacing values of 0.205 nm and 0.216 nm could be measured, which can be ascribed to Co (1 1 1) (PDF#15-0806) and PdCo alloy (1 1 1) (PDF#65-6075), respectively. Thus, PdCo alloy phase over Pd/CoO_x can be visually confirmed by HR-TEM. However, we failed in calculating the average particle size because it is difficult to find the boundary of PdCo

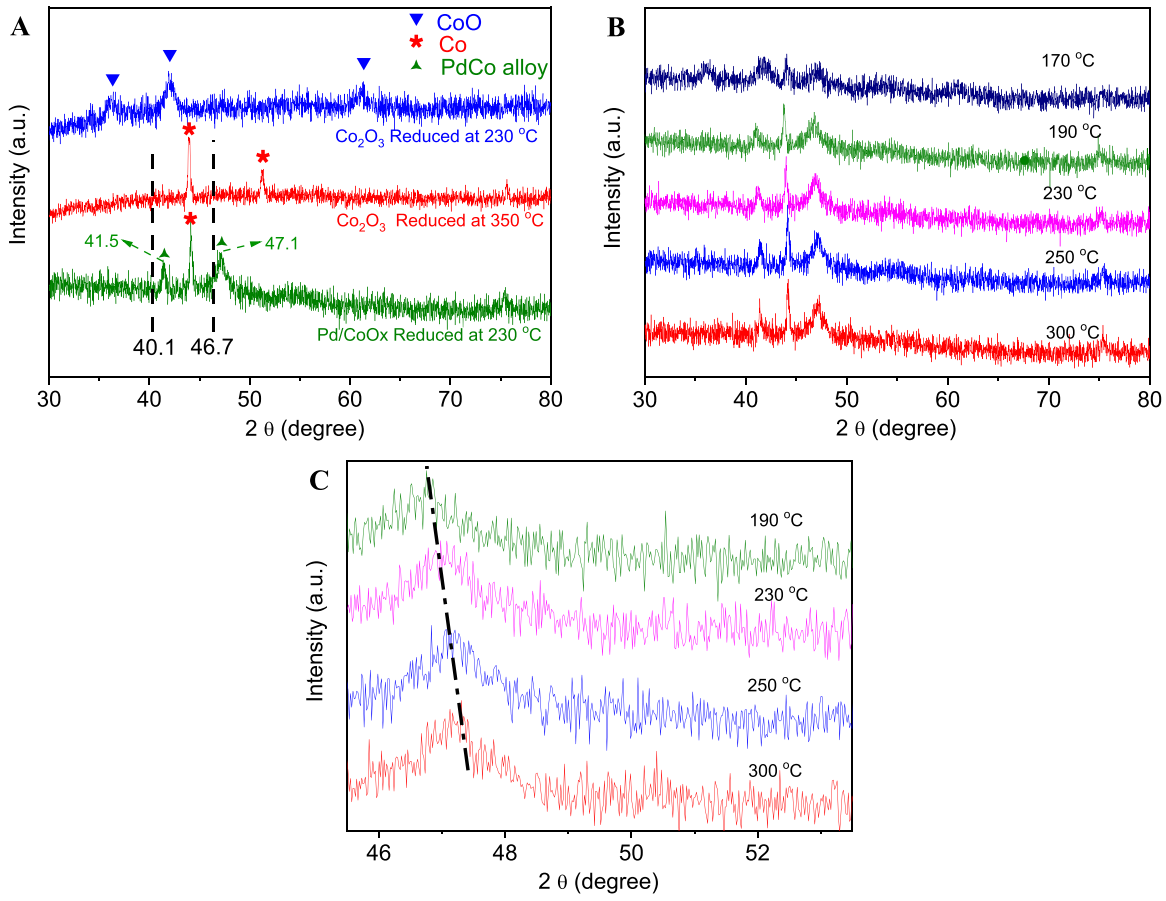

Fig. 4. XRD patterns of (A) Pd/CoO_x reduced at 230 °C and CoO_x reduced at 230 and 350 °C, (B) Pd/CoO_x reduced at different temperature in the full range, and (C) Pd/CoO_x reduced at different temperature in the (2 0 0) peak region.

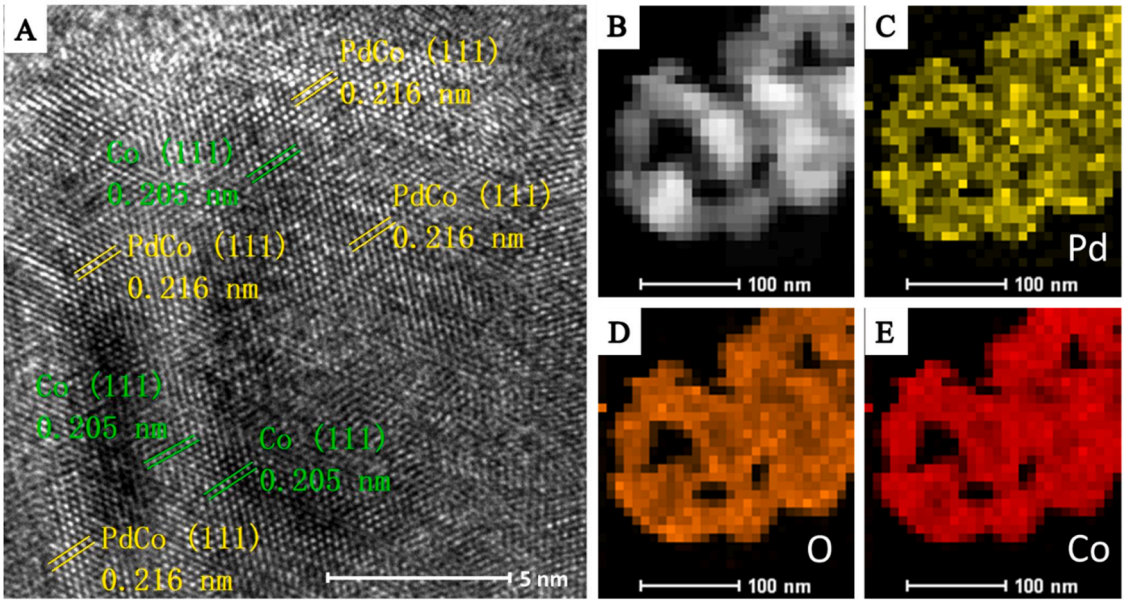

Fig. 5. (A) HR-TEM image, (B) HAADF-STEM image, and (C, D and E) mapping of Pd/CoO_x.

alloy particles in HR-TEM image. Besides, no pure Pd nanoparticle was found. To get more information of Pd distribution, HAADF-STEM picture and the corresponding mapping images were taken. Fig. 5C clearly illustrates that Pd element is homogeneously distributed over the whole catalyst particles. However, as can be seen Fig. 5A, PdCo alloy cannot be identified in most part of HR-TEM image. Thus, it can be deduced that there must be some well dispersed Pd that cannot be characterized by HR-TEM and also XRD, and the existing form of the well dispersed Pd remains unknown (Pd alone or PdCo alloy?).

H_2-TPR profiles of Pd/CoO_x and Co_2O_3 are shown in Fig. 6A. For

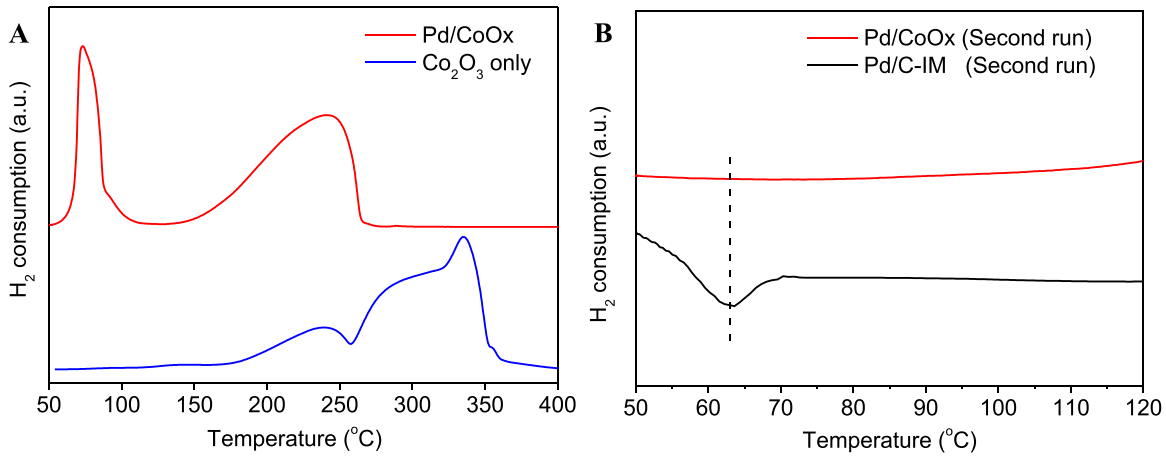

Fig. 6. (A) H_2-TPR profiles of Co_2O_3 and Pd/CoO_x; (B) second repeated H_2-TPR profiles of Pd/CoO_x and Pd/C-IM after reduction.

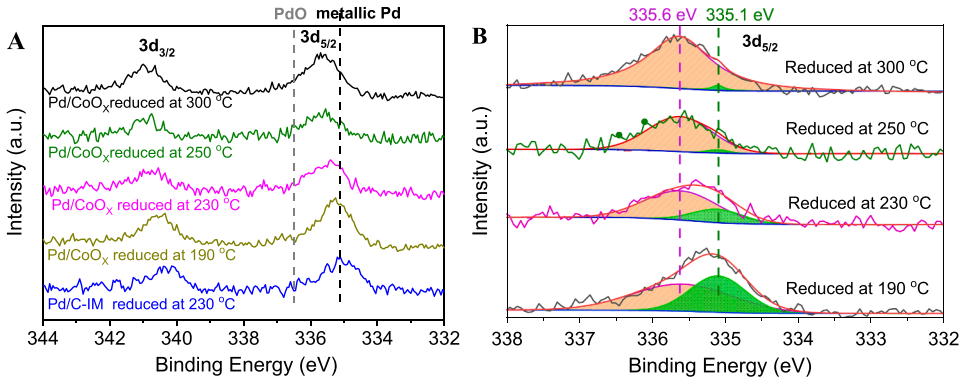

Fig. 7. (A) XPS spectrum of Pd 3d region in in situ reduced Pd/CoO_x and Pd/C-IM; (B) deconvolution of the Pd $3d_{5/2}$ peaks of reduced Pd/CoO_x catalysts.

Table 2
Relative peak areas of Pd species determined by deconvolution of the XPS spectra of reduced Pd/CoO_x samples.

Catalyst	Reduction temperature (°C)	Relative peak areas (%)	
		PdCo alloy (335.6)	Metallic Pd (335.1)
Pd/ CoO_x	300	98.1	1.9
	250	96.9	3.1
	230	76.8	23.2
	190	57.6	42.4

Table 3
Catalytic performance of 1,2- propanediol hydrogenolysis at 170 °C.[a]

Catalysts	Reduction temperature (°C)	Yield (%)		1,2-PDO Conversion (%)
		EtOH	NPA	
3%Pd/ CoO_x	190	2.25	0.20	2.54
	210	2.82	0.30	3.19
	230	4.19	0.47	4.88
	250	5.54	0.68	6.60
	300	5.43	0.83	6.83
Metallic Co[b]	350	1.12	4.41	7.10
3%Pd/C	230	0.61	0.13	0.83

[a] Reaction conditions: 0.25 g catalyst (before reduction), 10.9 mmol 1,2-PDO, 5 h, 3 MPa H_2, 170 °C.
[b] Metallic Co were obtained by reducing Co_2O_3 at 350 °C.

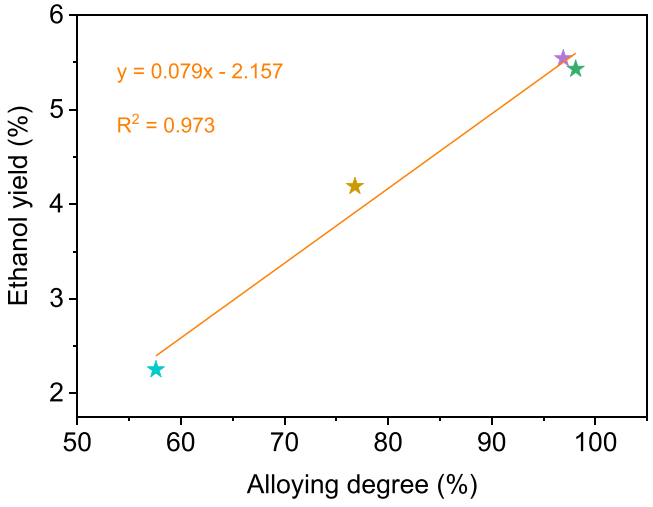

Fig. 8. Relationship between PdCo alloy degree obtained by XPS and ethanol yield listed in Table 3.

Co_2O_3, the reduction reaction started at about 170 °C. After raising the temperature to 360 °C, the Co_2O_3 sample was completely converted to metallic Co. In the case of Pd/ CoO_x, two separated peaks can be observed, and the finishing reduction temperature was shifted to 267 °C, much lower than Co_2O_3. It is interesting to note that the area ratio of second and first peak was 3.3: 1 in the H_2-TPR profiles of Pd/CoO_x (Fig. S1), much lower than the ratio of theoretical H_2 consumption value

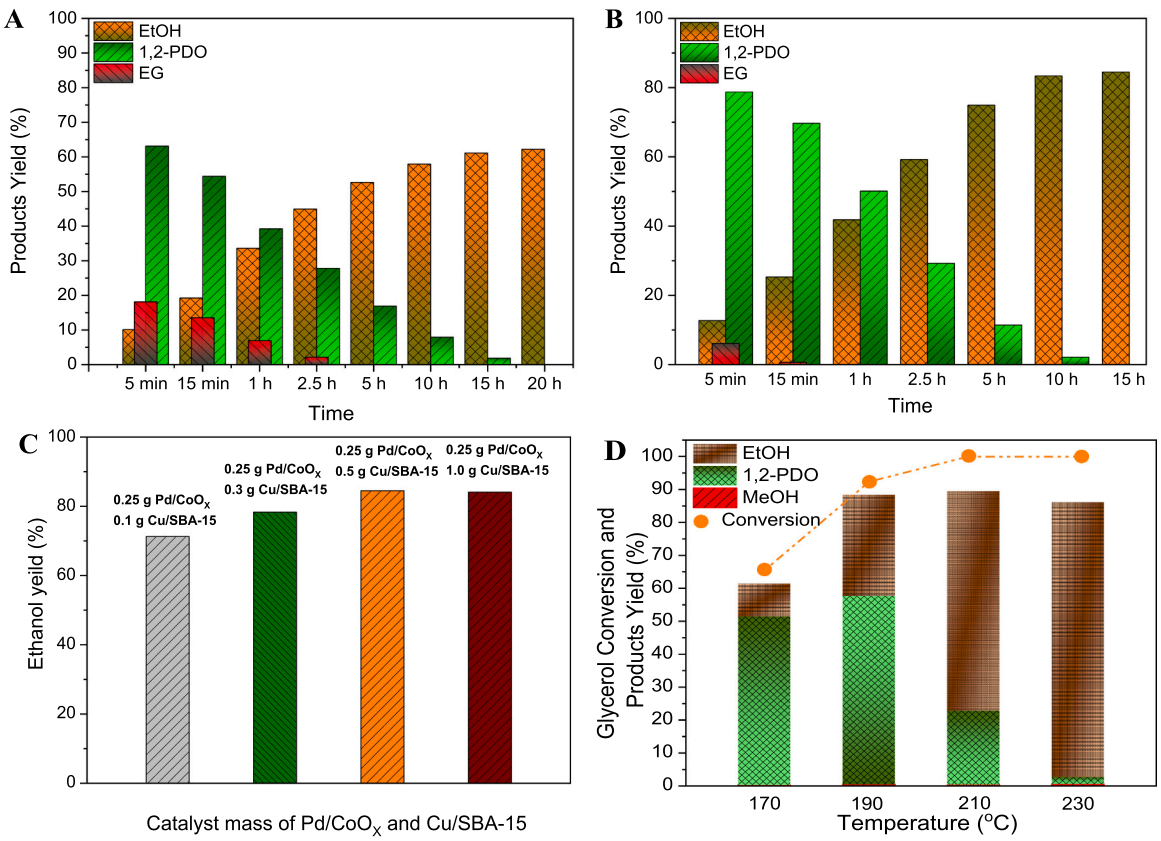

Fig. 9. Ethanol, EG and 1,2-propanediol yield at different reaction time over (A) 0.25 g Pd/CoO_x and (B) mixture of 0.25 g Pd/CoO_x and 0.5 g Cu/SBA-15. (C) Effect of Cu/SBA-15 amount on ethanol yield after 15 h reaction. (D) Effect of reaction temperature on glycerol conversion and products yield after 10 h reaction. Reaction conditions: 1 g (10.9 mmol) glycerol, 9 g 1-propanol, 3 MPa H_2, 230 °C.

Table 4
Liquid-phase product yield for 1,2-propanediol and ethylene glycol hydrogenolysis on Pd/CoO_x and the mixture of Pd/CoO_x and Cu/SBA-15 using 1-propanol as solvent.[a]

Catalyst	Time	Reactant	Conv. (%)	Yield, selectivity (%)	
				MeOH	EtOH
Pd/CoO_x[b]	15 min	1,2-PDO	16.5	0.4, 2.4	14.6, 88.5
	2 h		33.5	0.2, 0.5	27.3, 81.5
	15 h		98.9	0.4, 0.4	70.3, 71.1
Pd/CoO_x + Cu/SBA-15[c]	15 min	1,2-PDO	19.1	0.1, 0.5	17.5, 91.6
	2		48.0	0.2, 0.4	43.6, 90.8
	10		100	0.2, 0.2	88.7, 88.7
Pd/CoO_x[b]	1 h	EG	21.3	3.2, 15.0	6.2, 29.1
Pd/CoO_x + Cu/SBA-15[c]	1 h	EG	45.4	2.4, 5.3	30.9, 68.1

[a] Reaction conditions: 10.9 mmol 1,2-PDO/EG, 3 MPa H_2, 230 °C.
[b] 0.25 g catalyst was used in tests with Pd/CoO_x alone.
[c] The mixed catalysts were composed of 0.25 g Pd/CoO_x and 0.5 g Cu/SBA-15.

of Co_2O_3 and PdO (62: 1). Thus, part of carrier contributed to the formation of the first reduction peak, implying that the starting reduction temperature of the carrier might be lower than 100 °C in Pd/CoO_x. Above results suggest that the presence of Pd can dramatically facilitate the reduction of Co_2O_3, consistent with XRD characterization result that Co species were almost fully reduced to metallic Co in Pd/CoO_x at 230 °C while only diffraction peaks of CoO can be observed for Co_2O_3 reduced at the same temperature (Fig. 4A).

Fig. 6B clearly shows the absence of typical hydrogen evolution peak of β-Pd hydride [38,47] in the second TPR profile of the same Pd/CoO_x catalyst without exposure to air before the second TPR operation. For reduced pure Pd particles, hydrogen molecules should readily be absorbed to form Pd hydride at room temperature [38]. The formed Pd hydride will release hydrogen at elevated temperature, as displayed by the activated carbon-supported Pd sample (the negative peak centered at 63 °C). However, this phenomenon was not observed over Pd/CoO_x catalyst, as shown in Fig. 6B. This fact indicates that the formation of Pd hydride over reduced Pd/CoO_x catalyst is inhibited, most likely due to the formation of PdCo alloy leading to a strong metal-support interaction. The repeated TPR procedure helps better understanding of the existing form of the well dispersed Pd that cannot be distinguished by XRD and HR-TEM.

XPS analysis was used to determine the chemical states of Pd in Pd/CoO_x catalyst at different reduction temperature (Fig. 7A and Table S3). The Pd 3d region shows two peaks centered at binding energy values of about 335 and 340 eV, which should be assigned to the low-energy band (Pd $3d_{5/2}$) and high-energy band (Pd $3d_{3/2}$), respectively [44]. Fig. 7A clearly indicates that the binding energy of Pd $3d_{5/2}$ shows a positive shift in Pd/CoO_x samples as compared to Pd/C-IM, and the binding energy value of Pd $3d_{5/2}$ in Pd/C-IM sample is consistent with metallic Pd according to the former literatures [31]. It has been put forward that the positive binding energy shift of Pd $3d_{5/2}$ indicates alloy formation between Pd and other less noble metals such as Fe [38,44], Co [44–46, 48] and Cu [49,50]. And more notably, the binding energy value of Pd $3d_{5/2}$ got higher and higher in Pd/CoO_x with the reduction temperature rising from 190 to 250 °C, suggesting the increase in alloying degree

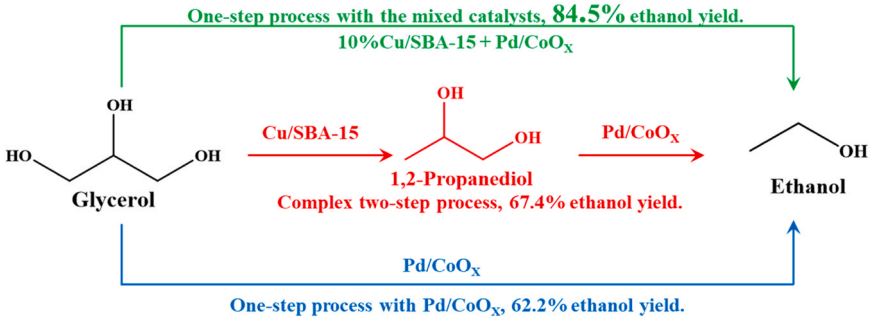

Scheme 2. Catalytic results for direct conversion of glycerol to ethanol over the mixed catalysts as well as Pd/CoO_x and by the two-step method.

with increasing reduction temperature [38]. For the XPS spectra of Pd/CoO_x samples reduced at 250 and 300 °C, the Pd 3d region shows little difference, suggesting that the alloying degree of the two samples are similar.

Above characterization results illustrates that almost all Pd atoms have interacted with the carrier to form PdCo alloy in Pd/CoO_x reduced at 250 °C or higher temperature. To get the numerical values of alloying degree, the Pd $3d_{5/2}$ peak of every reduced Pd/CoO_x sample was deconvoluted into two peaks centered at 335.1 and 335.6 eV, which are related to PdCo alloy and metallic Pd, respectively [44,45]. The fitting curves of Pd/CoO_x reduced at different temperature are shown in Fig. 7B, and the fitting parameters are shown in Table S4. The alloying degree is represented by the relative peak areas of PdCo alloy (Table 2).

Cu/SBA-15 used in this research is the same sample employed in our former report [5], and the corresponding characterization results are shown in Fig. S2.

3.3. Active center identification of Pd/CoO_x for glycerol conversion to ethanol

As discussed in part 3.1, Pd containing catalysts with supports except for Co_2O_3 showed low ethanol selectivity or catalytic stability (Fig. 1A and Fig. 2). Thus, the carrier plays an essential role for ethanol production. Compared to Pd, Pt and Ru supported on cobalt oxide prepared by co-precipitation also exhibited low selectivity to ethanol (Fig. 1B). Besides, high selectivity to ethanol was not achieved in reactions with Pd/C-IM as catalysts (Fig. 1A), suggesting that Pd alone was not the main active site for the transformation of glycerol to ethanol. Hence, the synergetic effect of Pd and cobalt oxide probably led to the production of ethanol as the primary product.

1,2-propanediol has been verified as the predominantly intermediate for ethanol production from glycerol on Pd/CoO_x in part 3.1. Since it is much more rapidly for glycerol hydrogenolysis to 1,2-propanediol than subsequent 1,2-propanediol conversion to ethanol, the active center in Pd/CoO_x for catalytic conversion of glycerol to ethanol can be distinguished by finding out the active site for the cleavage of C—C bond between two vicinal hydroxyl-linked carbon atoms in 1,2-propanediol.

The catalytic results of Pd/C-IM and metallic Co (Fig. 1) indicate that Pd or Co alone cannot convert glycerol to ethanol efficiently, so PdCo alloy in Pd/CoO_x probably acts as the active site for getting high yield of ethanol. To prove this, hydrogenolysis of 1,2-propanediol reactions were conducted with Pd/CoO_x catalysts reduced at 190, 210, 230, 250 and 300 °C, and the reaction temperature was set as 170 °C for every test. As shown in Tables 3, 1,2-propanediol conversion and ethanol yield were both promoted with the reduction temperature rising from 190 to 250 °C. It has been established by XPS in part 3.2 that alloying degree (relative amount of PdCo alloy) increased from 57.6% to 96.9% with the reduction temperature rising from 190 to 250 °C. Thus, a linear positive relationship can be obtained between ethanol yield and PdCo alloy degree, as shown in Fig. 8. However, the content of metallic Co might also increase with the rising of reduction temperature, so the role of Co should be confirmed. As seen in Table 3, metallic Co showed much higher selectivity to 1-propanol than ethanol in hydrogenolysis of 1,2-propanediol, and Pd/C-IM exhibited low reactivity despite the relative high ethanol selectivity. Thus, metallic Co and Pd cannot effectively catalyze glycerol to ethanol, and PdCo alloy can be definitely identified as the main active site for glycerol hydrogenolysis to ethanol.

Additionally, it can be found that further increase of reduction temperature to 300 °C led to a slight increase of 1,2-propanediol conversion and a little decrease of ethanol selectivity (Table 3). It has been well established that higher annealing temperature can result in more Co atoms incorporating into Pd lattice [46,51]. Although PdCo alloying degree did not change much for Pd/CoO_x with reduction temperature rising from 250 to 300 °C (Table 2), the incorporation of Co atoms to Pd lattice continued, as confirmed by the XRD patterns in Fig. 4C that the angle of PdCo alloy diffraction peak for Pd/CoO_x reduced at 300 °C is higher than that reduced at 250 °C. The continuing incorporation of Co atoms led to the decrease of surficial Pd/Co ratio, which was also evidenced by XPS (Table S5). Thus, the relative amount of surficial Co species increased with rising reduction temperature. As metallic Co showed higher reactivity and 1-propanol selectivity than Pd/CoO_x (Table 3 and Table S1), it should be reasonable that less ethanol was produced with elevated 1,2-propanediol conversion for Pd/CoO_x reduced at 300 °C.

3.4. Boosting ethanol selectivity by the assistance of Cu/SBA-15

As ethanol was mainly obtained via the 1,2-propanediol route and most ethylene glycol (another intermediate for ethanol production) was converted to methane, it is a good way to boost ethanol yield by increasing 1,2-propanediol production from glycerol or improving ethanol selectivity in ethylene glycol hydrogenolysis. Recently, we have shown that Cu/SBA-15 can efficiently catalyze glycerol to 1,2-propanediol with a selectivity higher than 98% because of large amounts of Cu^0 and adjacent Lewis acid sites [5]. Besides, the acid sites and Cu^0 surfaces together can also transform ethylene glycol to ethanol [52–55]. Thus, a catalyst system composed of Pd/CoO_x and Cu/SBA-15 might be applied for producing more ethanol from glycerol. Because Cu/SBA-15 showed poor stability in water [56,57] and Pd/CoO_x exhibited extremely low reactivity of glycerol hydrogenolysis to 1,2-propanediol with 1-propanol as reactant, 1-propanol was used as solvent in this part. The catalytic results are shown in Fig. 9 and Table S6. Glycerol conversion was 100% for all tests in Fig. 9 A–C.

Compared to reactions with water as solvent (Fig. 3), a slight promotion effect on reaction rate and ethanol selectivity can be observed when 1-propanol was employed as solvent. More notably, Pd/CoO_x gave an ethanol yield of 84.5% when 0.5 g Cu/SBA-15 was added. This value is much higher than the ethanol yield with Pd/CoO_x alone (62.2%) and also superior to the literature data (Table S7) [28–30]. As illustrated in Fig. 8A and B, addition of Cu/SBA-15 led to more 1,2-propanediol production from glycerol, so more ethanol could be obtained from the 1,2-propanediol route (Scheme 1). Besides, ethanol selectivity reached

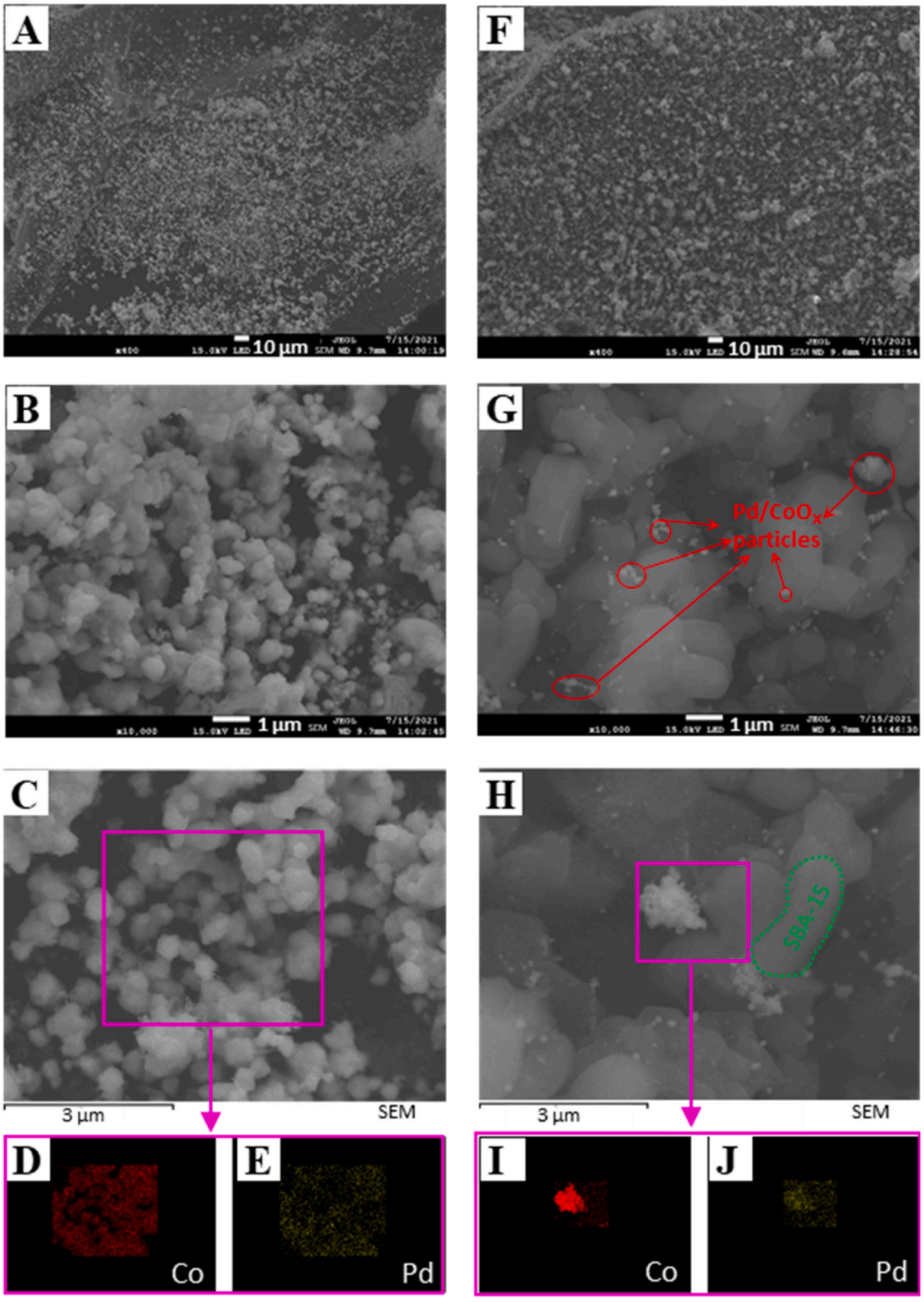

Fig. 10. (A–C) SEM images of Pd/CoO_x after three runs (the atomic number ratio of Co to Pd was obtained by ICP-AES); (D and E) mapping of the used Pd/CoO_x; (F–H) SEM images of the mixed catalysts (Pd/CoO_x + Cu/SBA-15) after three times reaction; (I and J) mapping of Pd/CoO_x in the used mixed catalysts.

68.1% for ethylene glycol hydrogenolysis on the mixed catalysts (Table 4). In contrast, on Pd/CoO_x, ethanol selectivity was only 29.1% at the same conditions. What's more, higher ethanol yield was also obtained in the transformation of 1,2-propanediol on the mixed catalysts than Pd/CoO_x (Table 4).

Above catalytic results have sufficiently proved that addition of Cu/SBA-15 can have a huge impact on the reaction routes of glycerol and ethylene glycol hydrogenolysis, leading to high ethanol yield from catalytic conversion of glycerol. Furthermore, the effects of Cu/SBA-15 amount and reaction temperature on glycerol conversion and ethanol

Table 5
Reusability results of catalytic conversion of glycerol to ethanol over the mixed catalysts composed of Pd/CoO_x and Cu/SBA-15.[a]

Sample	Glycerol conversion (%)						Ethanol selectivity (%)					
	1st run	2nd run	3rd run	4th[b] run	5th[c] run	6th[d] run	1st run	2nd run	3rd run	4th run	5th run	6th run
Pd/CoO_x + Cu/SBA-15	100	100	100	100	100	100	84.5	84.1	82.9	76.9	85.1	84.0

[a] Reaction conditions: 0.25 g Pd/CoO_x and 0.5 g Cu/SBA-15, 1 g (10.9 mmol) glycerol, 3 MPa H_2, 230 °C, 15 h.
[b] No fresh catalyst was added for the first four runs.
[c] Another 0.3 g fresh Cu/SBA-15 was added to the reaction system for the fifth run.
[d] The mixed catalysts obtained after the fifth run was employed without adding Cu/SBA-15.

selectivity have also been studied (Fig. 9C and D). There was an incremental impact of Cu/SBA-15 amount on ethanol yield. Addition of 0.5 g Cu/SBA-15 gave the optimum ethanol production, and further increase of Cu/SBA-15 amount made no difference. Besides, glycerol conversion and ethanol yield were remarkably promoted with the rising temperature in the range of 170–230 °C. In addition, a complex two-step method was also applied for glycerol conversion to ethanol. For the first step, 96.4% of glycerol was transformed to 1,2-propanediol by Cu/SBA-15. Thereafter, Pd/CoO_x continued to catalyze the second step in the separated solution and an ethanol yield of only 67.4% was obtained (Scheme 2).

However, there are still some phenomena that cannot be fully explained. It has been well documented that Cu/SiO_2 was not able to catalyze 1,2-propanediol to ethanol [3,10,58–61]. Additionally, as illustrated in Tables 4, 1,2-propanediol conversion reached 48.0% after 2 h on the mixed catalysts, but only 33.5% of the reactant was converted with Pd/CoO_x as catalyst. In this context, it remains unknown that how the addition of 10%Cu/SBA-15 promoted ethanol selectivity from 1, 2-propanediol and accelerated the reaction rate.

In order to make it clear, product distributions at different reaction time were analyzed for 1,2-propanediol hydrogenolysis over the mixed catalysts and pure Pd/CoO_x (Table 4). It can be found that there was only a slight difference in ethanol selectivity between the mixed catalysts (91.6%) and Pd/CoO_x (88.5%) at the initial stage. However, with reaction progress, ethanol selectivity experienced an obvious decrease on pure Pd/CoO_x and more 1-propanol was generated simultaneously. In contrast, the variation in ethanol selectivity was not pronounced on the mixed catalysts. This result suggests that the catalyst structures had changed a lot in reactions with Pd/CoO_x alone as catalyst. The SEM images of Pd/CoO_x after reaction just proves this point. As illustrated in Fig. 10B and G, after three reaction cycles, the catalyst powders size of pure Pd/CoO_x was much bigger than that of Pd/CoO_x in the mixed catalysts. The big crystals in Fig. 10G, and H were recognized as Cu/SBA-15 (Fig. S3). These results suggest that addition of Cu/SBA-15 can effectively suppress the aggregation of Pd/CoO_x powders and result in higher reactivity.

Furthermore, because metallic Co is favorable for 1-propanol production and PdCo alloy contributes to the generation of ethanol (Table S1 and Table 3), we speculate that the ratio of surficial PdCo alloy to exposed metallic Co declined along with the aggregation of Pd/CoO_x nanoparticles, which resulted in the lower ethanol yield over pure Pd/CoO_x. As shown in Table S5, the XPS results shows that surficial Pd/Co ratio in the used Pd/CoO_x sample was lower than that in the mixed catalysts. Furthermore, XRD patterns illustrate that more Co atoms incorporated to Pd lattice in pure Pd/CoO_x than the mixed catalysts during the reaction process (Fig. S4). Besides, ICP-AES was applied to determine the Pd/Co ratio of the whole catalyst, and only a slight decrease in the overall Pd/Co ratio was found for the used pure Pd/CoO_x sample (Table S5). Above results suggest that the decrease of surficial Pd/Co ratio by Co incorporation to Pd lattice in the aggregation process should be the primary reason for the lower selectivity to ethanol on pure Pd/CoO_x.

Moreover, the catalytic stability of mixed catalysts was tested. Table 5 gives glycerol conversion and ethanol selectivity in every reaction run. As can be seen, the mixed catalysts showed good reusability, with no obvious drop in ethanol yield after three reuse experiments. For the fourth run, ethanol selectivity dropped to 76.9% with 100% glycerol conversion. It should be noted that ethanol yield recovered to 85.1% after adding another 0.3 g fresh Cu/SBA-15 to the reaction system for the fifth reuse experiment. Moreover, no significant decrease in ethanol yield was observed in the sixth run. Above results suggest that the deactivation of Cu/SBA-15 should be the reason for the decrease in ethanol yield for the fourth run.

4. Conclusions

In summary, Pd/CoO_x prepared by co-precipitation was proved as a promising catalyst for consecutive hydrogenolysis of glycerol to ethanol, and high ethanol yield (57.8% in water and 62.2% in 1-propanol) was achieved. Catalytic results indicated that high ethanol selectivity was ascribed to the synergetic effect of Pd and the carrier in Pd/CoO_x. A well linear positive relationship has been obtained between ethanol yield and PdCo alloy degree. Thus, PdCo alloy was reasonably identified as the main catalytic active center for ethanol production from glycerol. More importantly, in couple with Cu/SBA-15, ethanol yield was greatly improved over Pd/CoO_x. Addition of Cu/SBA-15 not only adjusted the reaction routes of glycerol and ethylene glycol conversion, but also significantly slowed down the aggregation of Pd/CoO_x and kept its high selectivity to ethanol in the whole catalytic process. Finally, 84.5% yield of ethanol was achieved from glycerol hydrogenolysis by the cooperation of Pd/CoO_x and Cu/SBA-15, which is the highest ethanol yield ever reported in glycerol hydrogenolysis reactions.

CRediT authorship contribution statement

Jianfeng Shan: Conceptualization, Methodology, Investigation, Data curation, Writing – original draft. **Yanfeng Xue:** Methodology, Writing – review & editing. **Dengfeng Wang:** Supervision, Funding acquisition. **Zheng Chen:** Resources, Visualization. **Shanhui Zhu:** Conceptualization, Methodology, Writing – review & editing.

Declaration of Competing Interest

The authors declare that they have no competing interests.

Acknowledgements

The authors gratefully acknowledge financial support from the National Natural Science Foundation of China (21878321), the Key Research and Development Program of Shandong Province (2018GGX107010), the Natural Science Foundation of Shandong Province (ZR2020MB030, ZR2018LB030), the Natural Science Foundation for Youth Scholars of Shandong Province (ZR2020QB049), the Joint Fund of the Yulin University and the Dalian National Laboratory for Clean Energy (YLU-DNL Fund 2021005).

Appendix A. Supporting information

Supplementary data associated with this article can be found in the online version at doi:10.1016/j.apcatb.2021.120870.

References

[1] J. ten Dam, U. Hanefeld, Renewable chemicals: dehydroxylation of glycerol and polyols, ChemSusChem 4 (2011) 1017–1034.
[2] E.S. Vasiliadou, A.A. Lemonidou, Glycerol transformation to value added C3 diols: reaction mechanism, kinetic, and engineering aspects, WIREs Energy Environ. 4 (2015) 486–520.
[3] S. Zhu, X. Gao, Y. Zhu, Y. Zhu, H. Zheng, Y. Li, Promoting effect of boron oxide on Cu/SiO_2 catalyst for glycerol hydrogenolysis to 1,2-propanediol, J. Catal. 303 (2013) 70–79.
[4] C. Zhou, J.N. Beltramini, Y. Fan, G. Lu, Chemoselective catalytic conversion of glycerol as a biorenewable source to valuable commodity chemicals, Chem. Soc. Rev. 37 (2008) 527–549.
[5] J. Shan, H. Liu, K. Lu, S. Zhu, J. Li, J. Wang, W. Fan, Identification of the dehydration active sites in glycerol hydrogenolysis to 1,2-propanediol over Cu/SiO_2 catalysts, J. Catal. 383 (2020) 13–23.
[6] S. Zhao, W.D. Wang, L. Wang, W. Wang, J. Huang, Cooperation of hierarchical pores with strong Brønsted acid sites on SAPO-34 catalysts for the glycerol dehydration to acrolein, J. Catal. 389 (2020) 166–175.
[7] B. Ali, X. Lan, M.T. Arslan, H. Wang, S.Z.A. Gilani, S. Wang, T. Wang, Self-pillared MFI-Type zeolite nanosheets as selective catalysts for glycerol dehydration to acrolein, ACS Appl. Nano Mater. 3 (2020) 10966–10977.
[8] Z. Yuan, L. Wang, J. Wang, S. Xia, P. Chen, Z. Hou, X. Zheng, Hydrogenolysis of glycerol over homogenously dispersed copper on solid base catalysts, Appl. Catal. B: Environ. 101 (2011) 431–440.
[9] Y. Nakagawa, K. Tomishige, Heterogeneous catalysis of the glycerol hydrogenolysis, Catal. Sci. Technol. 1 (2011) 179–190.
[10] E.S. Vasiliadou, T.M. Eggenhuisen, P. Munnik, P.E. de Jongh, K.P. de Jong, A. A. Lemonidou, Synthesis and performance of highly dispersed Cu/SiO2 catalysts for the hydrogenolysis of glycerol, Appl. Catal. B: Environ. 145 (2014) 108–119.
[11] Y. Fan, S. Cheng, H. Wang, D. Ye, S. Xie, Y. Pei, H. Hu, W. Hua, Z. Hua, Li, M. Qiao, B. Zong, Nanoparticulate Pt on mesoporous SBA-15 doped with extremely low amount of W as a highly selective catalyst for glycerol hydrogenolysis to 1,3-propanediol, Green Chem. 19 (2017) 2174–2183.
[12] H. Zhao, L. Zheng, X. Li, P. Chen, Z. Hou, Hydrogenolysis of glycerol to 1,2-propanediol over Cu-based catalysts: a short review, Catal. Today 355 (2020) 84–95.
[13] G. Miao, L. Shi, Z. Zhou, L. Zhu, Y. Zhang, X. Zhao, H. Luo, S. Li, L. Kong, Y. Sun, Catalyst design for selective hydrodeoxygenation of glycerol to 1,3-propanediol, ACS Catal. 10 (2020) 15217–15226.
[14] K. Avasthi, A. Bohre, M. Grilc, B. Likozar, B. Saha, Advances in catalytic production processes of biomass-derived vinyl monomers, Catal. Sci. Technol. 10 (2020) 5411–5437.
[15] A. Kostyniuk, D. Bajec, P. Djinović, B. Likozar, Allyl alcohol production by gas phase conversion reactions of glycerol over bifunctional hierarchical zeolite-supported bi- and tri-metallic catalysts, Chem. Eng. J. 397 (2020), 125430.
[16] A. Kostyniuk, D. Bajec, P. Djinović, B. Likozar, One-step synthesis of glycidol from glycerol in a gas-phase packed-bed con- tinuous flow reactor over HZSM-5 zeolite catalysts modified by $CsNO_3$, Chem. Eng. J. 394 (2020), 124945.
[17] X. Zhang, S. Wei, X. Zhao, Z. Chen, H. Wu, P. Rong, Y. Sun, Y. Li, H. Yu, Preparation of mesoporous $CaO\text{-}ZrO_2$ catalysts without template for the continuous synthesis of glycerol carbonate in a fixed-bed reactor, Appl. Catal. A: Gen. 590 (2020), 117313.
[18] Y. Jiang, R. Zhou, H. Zhao, B. Ye, Y. Long, Z. Wang, Z. Hou, A highly active and stable organic-inorganic combined solid acid for the transesterification of glycerol under mild conditions, Chin. J. Catal. 42 (2021) 1772–1781.
[19] L. Yang, X. Li, P. Chen, Z. Hou, Selective oxidation of glycerol in a base-free aqueous solution: a short review, Chin. J. Catal. 40 (2019) 1020–1034.
[20] D. Sun, Y. Yamada, S. Sato, W. Ueda, Glycerol as a potential renewable raw material for acrylic acid production, Green Chem. 19 (2017) 3186–3213.
[21] A. Perosa, P. Tundo, Selective hydrogenolysis of glycerol with raney nickel, Ind. Eng. Chem. Res. 44 (2005) 8535–8537.
[22] E. van Ryneveld, A.S. Mahomed, P.S. van Heerden, M.J. Green, H.B. Friedrich, A catalytic route to lower alcohols from glycerol using Ni-supported catalysts, Green Chem. 13 (2011) 1819–1827.
[23] M.H. Haider, N.F. Dummer, D.W. Knight, R.L. Jenkins, M. Howard, J. Moulijn, S. H. Taylor, G.J. Hutchings, Efficient green methanol synthesis from glycerol, Nat. Chem. 7 (2015) 1028–1032.
[24] B. Chen, B. Zhang, Y. Zhang, X. Yang, Bimetallic effects of silver-modified nickel catalysts and their synergy in glycerol hydrogenolysis, ChemCatChem 8 (2016) 1929–1936.
[25] S. Sumari, F. Fajaroh, I.B. Suryadharma, A. Santoso, A. Budianto, Zeolite impregnated with Ag as catalysts for glycerol conversion to ethanol assisted by ultrasonic, IOP Conf. Ser.: Mater. Sci. Eng. 515, 2019, p. 012075.
[26] Y. Tang, Y. Huang, W. Gan, A. Xia, Q. Liao, X. Zhu, Ethanol production from gas fermentation: rapid enrichment and domestication of bacterial community with continuous CO/CO_2 gas, Renew. Energy 175 (2021) 337–344.
[27] M. Molaverdi, K. Karimi, S. Mirmohamadsadeghi, M. Galbe, High efficient ethanol production from corn stover by modified mild alkaline pretreatment, Renew. Energy 170 (2021) 714–723.
[28] L. Zheng, H. Zhao, J. Fu, X. Lu, Z. Hou, Direct production of ethanol from glycerol over Ni-substituted stichtite derived catalysts, Appl. Clay Sci. 153 (2018) 54–60.
[29] H. Zhao, Y. Jiang, P. Chen, J. Fu, X. Lu, Z. Hou, CoZn-ZIF-derived $ZnCo_2O_4$-framework for the synthesis of alcohols from glycerol, Green Chem. 20 (2018) 4299–4307.
[30] A. Kostyniuk, D. Bajec, B. Likozar, One-step synthesis of ethanol from glycerol in a gas phase packed bed reactor over hierarchical alkali-treated zeolite catalyst materials, Green Chem. 22 (2020) 753–765.
[31] C. Mota, B. Peres Pinto, A.L. de Lima, Glycerol: A Versatile Renewable Feedstock for the Chemical Industry, Springer International Publishing, 2017.
[32] N. Vikromvarasiri, S. Haosagul, S. Boonyawanich, N. Pisutpaisal, Microbial dynamics in ethanol fermentation from glycerol, Int. J. Hydrogen Energy 41 (2016) 15667–15673.
[33] V. Sawasdee, N. Vikromvarasiri, N. Pisutpaisal, Optimization of ethanol production from co-substrate of waste glycerol and acetic acid by Enterobacter aerogenes, Biomass Conv. Bioref. (2021).
[34] J. Sunarno, P. Prasertsan, W. Duangsuwan, B. Cheirsilp, K. Sangkharak, Improve biotransformation of crude glycerol to ethanol of Enterobacter aerogenes by two-stage redox potential fed-batch process under microaerobic environment, Biomass Bioenergy 134 (2020), 105503.
[35] J. Sunarno, P. Prasertsan, W. Duangsuwan, B. Cheirsilp, K. Sangkharak, Biodiesel derived crude glycerol and tuna condensate as an alternative low-cost fermentation medium for ethanol production by Enterobacter aerogenes, Ind. Crop. Prod. 138 (2019), 111451.
[36] I. Loaces, C. Rodríguez, V. Amarelle, E. Fabiano, F. Noya, Improved glycerol to ethanol conversion by E. coli using a metagenomic fragment isolated from an anaerobic reactor, J. Ind. Microbiol. Biot. 43 (2016) 1405–1416.
[37] M.S. Wong, M. Li, R.W. Black, T.Q. Le, S. Puthli, P. Campbell, D.J. Monticello, Microaerobic conversion of glycerol to ethanol in Escherichia coli, Appl. Environ. Microb. 80 (2014) 3276–3282.
[38] C.T. Wu, K.M.K. Yu, F. Liao, N. Young, P. Nellist, A. Dent, A. Kroner, S.C.E. Tsang, A non-syn-gas catalytic route to methanol production, Nat. Commun. 3 (2012) 1050.
[39] R. Burch, A.R. Flambard, Strong metal-support interactions in nickel/titania catalysts: the importance of interfacial phenomena, J. Catal. 78 (1982) 389–405.
[40] J. Luo, D. Chen, X. Yue, Y. Feng, Z. Huang, Study on syngas methanation over municipal solid waste char supported Ni catalyst, Fuel 303 (2021), 121222.
[41] Q. Wang, Y. Gao, C. Tumurbaatar, T. Bold, F. Wei, Y. Dai, Y. Yang, Tuned selectivity and enhanced activity of CO_2 methanation over Ru catalysts by modified metal-carbonate interfaces, J. Energy Chem. 64 (2022) 38–46.
[42] S. Ronsch, J. Schneider, S. Matthischke, M. Schluter, M. Gotz, J. Lefebvre, P. Prabhakaran, S. Bajohr, Review on methanation - from fundamentals to current projects, Fuel 166 (2016) 276–296.
[43] M. Vondrova, T. Klimczuk, V.L. Miller, B.W. Kirby, N. Yao, R.J. Cava, A. B. Bocarsly, Supported superparamagnetic Pd/Co alloy nanoparticles prepared from a silica/cyanogel Co-gel, Chem. Mater. 17 (2005) 6216–6218.
[44] F. Mauriello, H. Ariga, M.G. Musolino, R. Pietropaolo, S. Takakusagi, K. Asakura, Exploring the catalytic properties of supported palladium catalysts in the transfer hydrogenolysis of glycerol, Appl. Catal. B: Environ. 166–167 (2015) 121–131.
[45] L. Liu, G. Samjeske, S. Nagamatsu, O. Sekizawa, K. Nagasawa, S. Takao, Y. Imaizumi, T. Yamamoto, T. Uruga, Y. Iwasawa, Dependences of the oxygen reduction reaction activity of Pd–Co/C and Pd–Ni/C alloy electrocatalysts on the nanoparticle size and lattice constant, Top. Catal. 57 (2014) 595–606.
[46] L. Zhang, K. Lee, J. Zhang, Effect of synthetic reducing agents on morphology and ORR activity of carbon-supported nano-Pd–Co alloy electrocatalysts, Electrochim. Acta 52 (2007) 7964–7971.
[47] C.M. Mendez, H. Olivero, D.E. Damiani, M.A. Volpe, On the role of Pd β-hydride in the reduction of nitrate over Pd based catalyst, Appl. Catal. B: Environ. 84 (2008) 156–161.
[48] M. Wakisaka, S. Mitsui, Y. Hirose, K. Kawashima, H. Uchida, M. Watanabe, Electronic structures of Pt−Co and Pt−Ru alloys for CO-tolerant anode catalysts in polymer electrolyte fuel cells studied by EC−XPS, J. Phys. Chem. B 110 (2006) 23489–23496.
[49] C. Goswami, H. Saikia, B. Jyoti Borah, M. Jyoti Kalita, K. Tada, S. Tanaka, P. Bharali, Boosting the electrocatalytic activity of Pd/C by Cu alloying: insight on Pd/Cu composition and reaction pathway, J. Colloid Interfaces Sci. 587 (2021) 446–456.
[50] L. Wang, J.-J. Zhai, K. Jiang, J.-Q. Wang, W.-B. Cai, Pd–Cu/C electrocatalysts synthesized by one-pot polyol reduction toward formic acid oxidation: structural characterization and electrocatalytic performance, Int. J. Hydrogen Energy 40 (2015) 1726–1734.
[51] H. Liu, W. Li, A. Manthiram, Factors influencing the electrocatalytic activity of $Pd_{100-x}Co_x$ ($0 \leq x \leq 50$) nanoalloys for oxygen reduction reaction in fuel cells, Appl. Catal. B: Environ. 90 (2009) 184–194.
[52] Y. Zhu, X. Kong, X. Li, G. Ding, Y. Zhu, Y.-W. Li, Cu nanoparticles inlaid mesoporous Al_2O_3 as a high-performance bifunctional catalyst for ethanol synthesis via dimethyl oxalate hydrogenation, ACS Catal. 4 (2014) 3612–3620.
[53] Y. Zhu, X. Kong, S. Zhu, F. Dong, H. Zheng, Y. Zhu, Y.-W. Li, Construction of Cu/ZrO2/Al2O3 composites for ethanol synthesis: synergies of ternary sites for cascade reaction, Appl. Catal. B: Environ. 166–167 (2015) 551–559.
[54] Y. Zhu, Y. Zhu, G. Ding, S. Zhu, H. Zheng, Y. Li, Highly selective synthesis of ethylene glycol and ethanol via hydrogenation of dimethyl oxalate on Cu catalysts: influence of support, Appl. Catal. A: Gen. 468 (2013) 296–304.
[55] J. Shi, Y. He, K. Ma, S. Tang, C. Liu, H. Yue, B. Liang, Cu active sites confined in MgAl layered double hydroxide for hydrogenation of dimethyl oxalate to ethanol, Catal. Today 365 (2021) 318–326.
[56] Z. Chen, H. Ge, P. Wang, J. Sun, M. Abbas, J. Chen, Insight into the deactivation mechanism of water on active Cu species for ester hydrogenation: experimental and theoretical study, Mol. Catal. 488 (2020), 110919.

[57] S. Zhu, X. Gao, Y. Zhu, Y. Zhu, H. Zheng, Y. Li, Promoting effect of boron oxide on Cu/SiO_2 catalyst for glycerol hydrogenolysis to 1,2-propanediol, J. Catal. 303 (2013) 70–79.
[58] M. Harisekhar, V. Pavan Kumar, S. Shanthi Priya, K.V. Chary, Vapour phase hydrogenolysis of glycerol to propanediols over Cu/SBA-15 catalysts, J. Chem. Technol. Biotechnol. 90 (2015) 1906–1917.
[59] Z. Huang, F. Cui, J. Xue, J. Zuo, J. Chen, C. Xia, Cu/SiO2 catalysts prepared by hom- and heterogeneous deposition–precipitation methods: Texture, structure, and catalytic performance in the hydrogenolysis of glycerol to 1,2-propanediol, Catal. Today 183 (2012) 42–51.
[60] K.-T. Li, C.-H. Wang, H.-C. Wang, Hydrogenolysis of glycerol to 1,2-propanediol on copper core-porous silica shell-nanoparticles, J. Taiwan Inst. Chem. Eng. 52 (2015) 79–84.
[61] E.S. Vasiliadou, A.A. Lemonidou, Kinetic study of liquid-phase glycerol hydrogenolysis over Cu/SiO2 catalyst, Chem. Eng. J. 231 (2013) 103–112.